Teleoperated Touch Feedback from the Surfaces at the Nanoscale: Modelling and Experiments

Metin Sitti, *Member, IEEE,* and Hideki Hashimoto, *Member, IEEE*

***Abstract*— In this paper, a teleoperated nanoscale touching system is proposed, and continuum nanoscale contact mechanics models are introduced. The tele-nanorobotic system consists of a piezoresistive nanoprobe with a sharp tip as the nanorobot and force and topology sensor, a custom-made 1 degree of freedom haptic device for force-feedback, 3-D Virtual Reality graphics display of the nano world for visual feedback, and force-reflecting servo type scaled teleoperation controller. Using this system, 1-D and 3-D touching experiments and Virtual Reality simulations are realized. Scaling of nanoforces is one of the major issues of the scaled teleoperation system since nanometer scale forces are dominated by surface forces instead of inertial forces as in the macro world. As the force scaling approach, a heuristic rule is introduced where nanoforces are linearly scaled with an experimentally determined scaling parameter. Simulation results and preliminary experiments of touching to silicon and InAs quantum dot nanostructures show that adhesion forces at the nanoscale can be felt repeatedly at the operator's hand, and the proposed system can successfully enable the nanoscale surface topography and contact and non-contact nanoforce feedback.**

***Index Terms*— Nanorobotics, nanomanipulation, nanotechnology, nanomechanics, tele-robotics, haptic feedback.**

I. Introduction

HANDLING of and interacting with smaller and smaller size objects where the human sensing, precision, and direct manipulation capabilities lack is one of the promising future trends in the robotics field. Due to the recent developments in the nanotechnology field, handling of materials especially at the molecular and nanometer scales has become a new challenging issue [1], [2], [3], [4], [5]. On one side, some researchers are trying to understand more about the nano world physics and chemistry, and, on the other side, robotics researchers are attempting to construct new tools, new control and sensing technologies, and human-machine interfaces specific to the nano world. This study is focused on using Atomic Force Microscope (AFM) nanoprobes for teleoperated physical interactions and manipulation at the nanoscale. These nanoprobes can be utilized for different interaction and manipulation tasks as illustrated in Figure 1 [6]. This paper investigates the touching interaction applications in particular, but the developed approach could also be directly extended to other tasks. Most nanorobotics studies do not include the detailed effect of object deformation during contact type of manipulation. However, this study also introduces deformation and indentation models for understanding the nanoscale contact behavior in more detail.

M. Sitti is with the Carnegie Mellon University, Department of Mechanical Engineering and the Robotics Institute, Pittsburgh, USA. E-mail: msitti@andrew.cmu.edu

H. Hashimoto is with the Institute of Industrial Science, University of Tokyo, Japan.

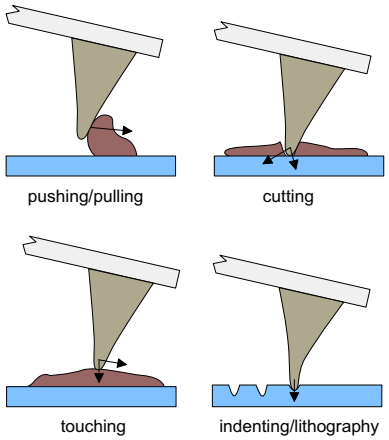

Fig. 1. Possible mechanical manipulation tasks using an AFM probe as a nanomanipulator.

When the objects are scaled down to the nanometer scale, there are many significant changes in the physics and properties of materials: (1) surface-to-volume ratio increases, i.e. surface forces, friction and drag forces dominate inertial forces, surface properties could dominate bulk properties, and friction becomes also a function of contact area, (2) dynamics of the objects becomes faster, (3) heat dissipation increases, etc. Thus, a different mechanics, which can be called as *nanomechanics*, is introduced by many researchers [7], and nanoscale contact mechanics [8] is one of the main components of this new field. For understanding the contact phenomenon of surface atoms and molecules at the nanoscale, Surface Force Apparatus and more recently Atomic Force Microscope (AFM) have been utilized [9], [10] as experimental tools intensively. AFM can enable single asperity contact studies of any type of sample such as biological objects, polymers, metals, semi-conductors, etc. Thus, local contact studies with very high resolution has become possible. For AFM-based contact mechanics modelling, two main approaches are used: molecular dynamics simulations and continuum mechanics. In the former approach, interatomic molecular dynamic models are utilized for numerically calculating the dynamics of each atom on the indenter and the surface [11]. On the other hand, the continuum mechanics approach generates the contact mechanics by integrating the interatomic forces at each body. For basic nanorobotic applications, the continuum mechanics approach is advantageous since it is analytical and computationally efficient while the former is crucial for understanding the molecular basis of contact mechanics. The continuum mechanics approach is selected in this paper because the models are aimed to be utilized in real-time haptic interfaced

Virtual Reality (VR) simulations.

Hertz [12], [13], [14], [15], Johnson-Kendall-Roberts (JKR) [16], Derjaguin-Muller-Toporov (DMT), Maugis-Dugdale (MD) [17], [18], etc. models have been utilized as the continuum mechanics approaches. The Hertz model is realistic when the external loads are much larger than the adhesion forces. However, load amounts may have similar magnitudes to adhesion forces during nanomanipulation tasks, thus this model should not be utilized in the case of small loads. The DMT model adds the effect of adhesion to the Hertz model, and it can be used in the case of rigid systems, low adhesion, and small radii of curvature. But it may underestimate the true contact area, and the hysteresis between loading and unloading cannot be modeled with this model. On the other hand, the JKR model includes the effect of adhesion forces and hysteresis behavior where it is realistic for small loads. But, it assumes that short-ranged surface forces act only inside the contact area, and this may underestimate loading due to the surface forces. Finally, the MD model [19] is currently the best model since it can be used for any case and does not underestimate surface forces and contact area.

In this paper, nanoscale contact mechanics is connected with the scaled tele-robotics technology for putting human operators *inside* the nano world for touching and physically interacting with surfaces at the nanoscale. This kind of study is especially crucial for reliable tele-manipulation of fragile, soft and complex nanoobjects such as biological samples or polymers. This paper integrates nanoscale contact mechanics and teleoperated force and topography feedback for the first time to our knowledge. Hollis et al. [20] and Falvo et al. [21] utilized tele-robotics technology for tele-manipulation or tactile feedback, but did not consider the nanoscale contact mechanics and scaled teleoperation control design issues in detail.

Our approach is to utilize Hertz, DMT, JKR, and MD contact models in a Virtual Reality based nanoscale touching simulator for an AFM nanoprobe contact interaction with surfaces, and then compare the results with teleoperated AFM nanoprobe touching experiments. For the bilateral teleoperation force feedback control, a force-reflecting servo-type controller is used. The scaling problem for this kind of application is defined, and possible solutions are proposed.

The organization of the paper is as follows: after defining the nanoscale touch feedback problem in Section II, nanoscale force models and contact mechanics are described in Section III. Then, scaled bilateral teleoperation control and force scaling approaches are given in Section IV. Next, Section V explains the VR graphics environment for teleoperated nanoscale touch simulations and experiments. Simulations and experimental results of the teleoperated touch system are reported in Section VI, and Section VII and VIII include discussions of these results and conclusions respectively.

II. Problem Definition

AFM cantilever with its sharp tip as shown in Figure 2 is replaced by our finger at the nanoscale as shown in Figure 3. The operations are assumed to be realized in ambient conditions with no direct humidity and temperature control for the AFM system. Here, the sample is assumed to be an elastic flat half-space, and the cantilever beam is assumed to be a point mass concentrated on the tip apex with a spring and damper.

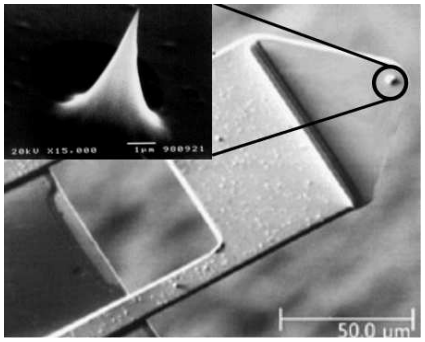

Fig. 2. Bottom view of the piezoresistive AFM nanoprobe (Thermomicroscopes Inc.) [22] by Scanning Electron Microscope where the silicon tip (inner image) with apex radius of $20-30\ nm$ is located around $10\ \mu m$ inside of the end.

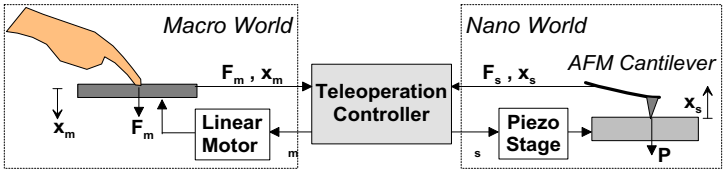

Fig. 3. Contact-type physical interaction with deformable surfaces at the nanoscale using AFM tip as a single asperity contact tool and force/topology sensor.

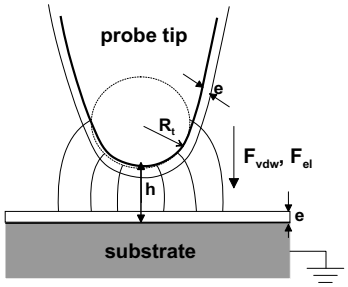

Fig. 4. A parabolic nanoprobe tip and a flat surface interacting via the van der Waals, electrostatic and capillary forces.

III. Continuum Nanoforce Models

Assuming the AFM tip apex is spherical (parabolic), nanoforces between a sphere and an elastic flat surface, as illustrated in Figure 4, are to be modelled for simulating the touch interaction in a VR environment. An experimental force-distance curve of a silicon tip and silicon surface in ambient conditions is shown in Figure 5. During approach, there is a non-contact force which starts at around $40\ nm$ distance at point **A** for this case, and attracts the probe to the surface. Then the tip contacts the surface, and after this point contact forces repel the tip depending on the contact mechanics. When the tip retracts, there is a hysteresis, and adhesion peak after point **B**, and the tip and surface are completely detached at point **C**.

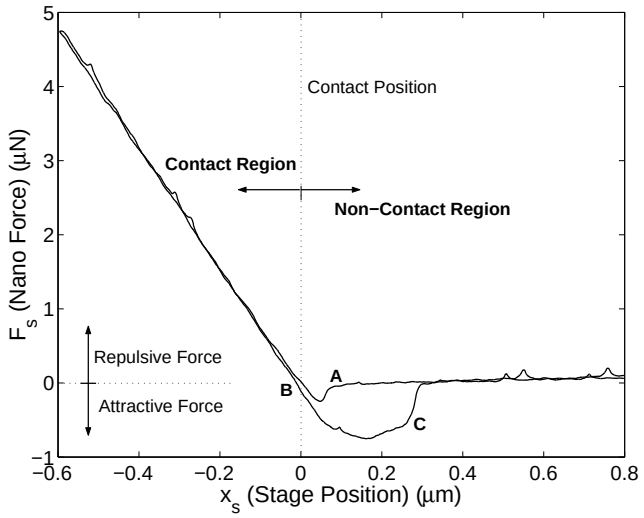

Fig. 5. Experimental force-distance curve during approach to and retraction from a flat silicon surface with the piezoresistive AFM nanoprobe.

Below, the main forces causing the non-contact attraction and contact repulsion are modelled and explained.

A. Non-Contact Forces

While approaching or retracting, there are mainly attractive and sometimes repulsive non-contact forces in ambient conditions (gravitational forces are negligible relative to the other nanoforces). These forces are mainly van der Waals, capillary and electrostatic forces such that $F_{non-con}(t) = F_{vdw}(t) + F_{cap}(t) + F_{el}(t)$. For these forces, a minus sign represents attractive and a plus sign does repulsive force cases. Assuming a spherical (semi)conducting tip of radius R_t, and (semi)conducting flat surface separated by a distance h and peak-to-peak surface roughness b, these forces are given as follows [23], [4]:

$$\begin{aligned} F_{vdw}(h) &= -\Big(\frac{h}{h+b/2}\Big)^2 \frac{HR_t}{6h^2}\ ,\ (h \le 100\ nm) \\ F_{cap}(h) &\approx -4\pi\gamma_L R_t\Big(1-\frac{h-2e}{2r_1}\Big)\ , \\ F_{el}(h) &= -\frac{\epsilon_0 U^2 S}{2h^2}\ ,\ (h \ge a_0) \end{aligned} \tag{1}$$

H is the Hamaker constant, r_1 is the radius of curvature of the meniscus, e is the thickness of the liquid layer, γ_L is the water surface energy, ϵ_0 is the permittivity, $U = (\phi_1 - \phi_2)/e_c$ where ϕ_1 and ϕ_2 are the work functions of two surfaces, and $e_c = 1.6 \times 10^{-19}\ C$ is the electron charge, $S = 4\pi R_t r_1$ is the contact area, and a_0 is the interatomic distance between the tip and surface atoms. Here, the surface roughness (b) is very significant since the surfaces at the nanometer scale are mostly not atomically flat. As can be seen from the above F_{vdw} equation, b can exponentially decrease the surface forces.

1) Simulations: The above non-contact force models are simulated, and their relative magnitudes in air are compared. For approaching a spherical silicon tip to a flat gold surface, the parameters of the simulation are as follows: $R_t = 30\ nm$, $H = 2.03 \times 10^{-19}\ J$, $a_0 = 1.98\ A^o$, $e = 5\ nm$, $b \approx 0$, $\gamma_L = 72\ mJ/m^2$, $r_1 = 1.06\ nm$, $U = 0.25\ V$, $\epsilon_0 = 8.85 \times 10^{-12}\ C^2/Nm^2$. The resulting forces are shown in Figure 6. From the figure it can be seen that $F_{cap} > F_{vdw} > F_{el}$ for the given case. F_{cap} dominates F_{vdw} in air for hydrophilic surfaces since they always have a thin water layer in ambient conditions, and F_{el} could be neglected if the surface is (semi)conducting and grounded while this does not hold for nonconductive or previously charged surfaces.

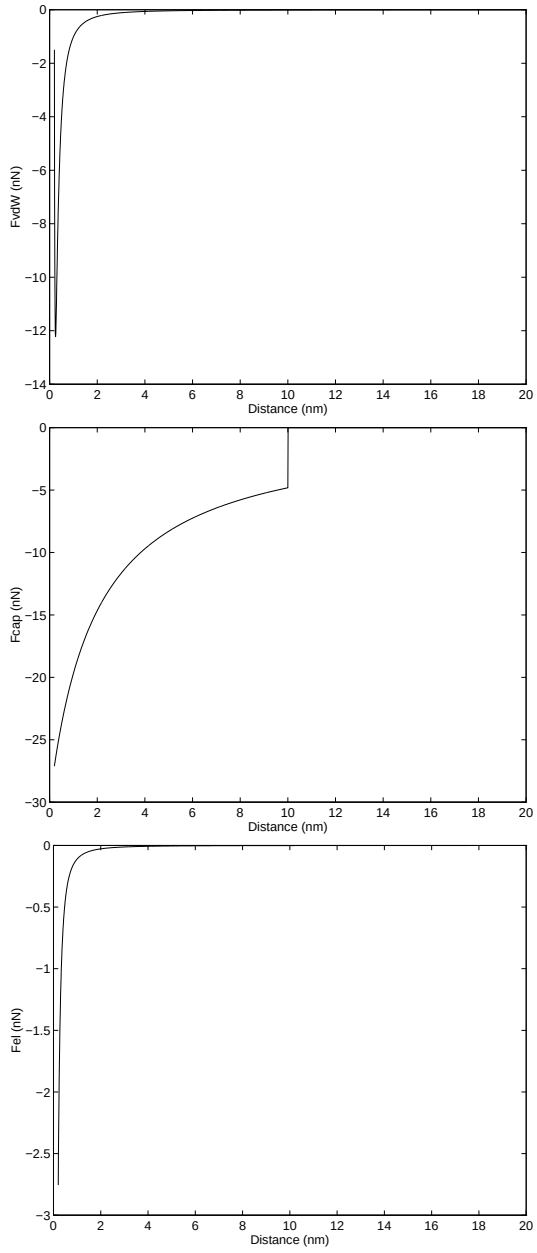

Fig. 6. Comparison of the magnitudes of the F_{vdw} (uppermost), F_{cap} (middle) and F_{el} (bottom) non-contact attractive forces in air for a silicon tip and gold substrate.

B. Contact Mechanics

The contact mechanics of the nanoscale touch using the AFM tip as the single asperity contact tool is modelled as a mass-spring system as shown in Figure 7. P represents the

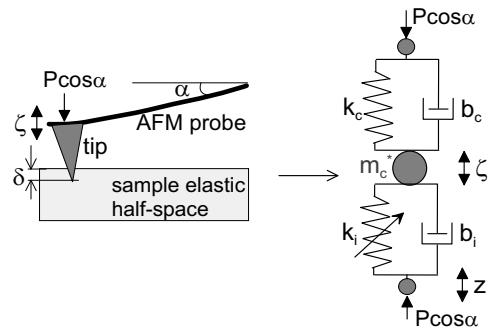

Fig. 7. Mass-spring model of the contact mechanics for the elastic surfaces at the nanoscale using AFM tip as a single asperity contact tool.

applied load, k_c, b_c, m_c, ζ are the cantilever force constant, damping constant, mass, and deflection respectively. $k_i(z,\zeta)$ and b_i are the tip-surface interaction stiffness and damping, and δ is the penetration depth. The dynamics of the cantilever can be given as [7]:

$$\begin{aligned} m_c^*\ddot{\zeta}(t) + 2m_c^* b_c \dot{\zeta}(t) + k_c\zeta(t) = \\ k_i(z,\zeta)(z(t)-\zeta(t)) + 2m_c^* b_i(\dot{z}(t)-\dot{\zeta}(t) \ , \end{aligned} \tag{2}$$

where $m_c^* = 0.24m_c$ is the effective mass for a rectangular probe. Assuming the damping terms are negligible, and removing the time $t \in R$ for the notation simplicity:

$$m_c^*\ddot{\zeta} + k_c\zeta = k_i(z,\zeta)(z-\zeta) \ . \tag{3}$$

Here, the special cases are: (1) if $k_i >> k_c$, $\zeta = z$ at the equilibrium which means there is no surface deformation, (2) when $k_i = -k_c$, i.e. k_i is due to an attractive tip-sample interaction force F_i with $k_i = dF_i/dz = -k_c$, then $m_c^*\ddot{\zeta} = k_i z$. During the contact, applying a load P by moving the cantilever base position to z results in the following equalities:

$$\begin{aligned} P(t) &= k_c\zeta(t) \\ \delta(t) &= \Delta(t) - \zeta(t)cos\alpha \\ \Delta(t) &= z(t) - z_0 \ , \end{aligned} \tag{4}$$

where z_0 is the stage z-position when the tip contacts to the sample and Δ is the stage z-displacement from z_0 after the tip-sample contact.

1) Hertz Model: For the Hertz contact model as shown in Figure 8a, load P results in a contact radius a with the general relation of:

$$\begin{aligned} P &= Ka\delta \\ \frac{1}{K} &= \frac{m}{2}\Big(\frac{1-\nu_t^2}{E_t} + \frac{1-\nu_s^2}{E_s}\Big) \end{aligned} \tag{5}$$

where K is the *reduced elastic modulus* for the tip-sample system, m is the tip geometry dependent constant ($m = 1$ for the cylindrical, $m = 1.5$ for the spherical, and $m = 2$ for the conical tip case), E_t and E_s are the Young's moduli, and ν_t and ν_s are the sample Poison's coefficients respectively. For our system, the AFM tip is spherical with radius $R_t \approx 20-30\ nm$, and using the Hertz model for a sphere-flat object interaction, $a = \sqrt{R_t\delta}$ assuming small deformation. Then, the following relation can be computed:

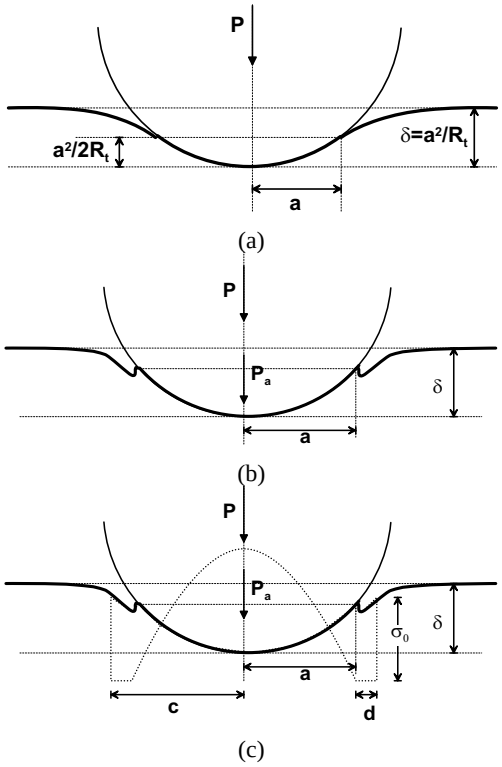

Fig. 8. Contact mechanics models for an elastic sphere and flat surface case for a load of P and adhesion force of P_a: (a) the Hertz model, (b) the JKR model, (c) the MD model.

$$\Delta = \delta + \frac{\sqrt{R_t}Kcos\alpha}{k_c}\delta^{3/2} \ . \tag{6}$$

If the tip is very sharp, i.e. $R_t < 10\ nm$, the geometry can be assumed to be conical with the tip half angle ψ where $a = \pi tan\psi\delta/2$. Then,

$$\Delta = \delta + \frac{\pi tan\psi}{2Kk_c}\delta^2 \ . \tag{7}$$

Furthermore, some researchers [14] approximate the contact radius using simple geometry as $a \approx \sqrt{2\Delta R_t}$ for the spherical tip case, then:

$$\delta = \frac{k_c\Delta}{k_c + Kcos\alpha\sqrt{2\Delta R_t}} \ . \tag{8}$$

2) DMT Model: This model accounts for long-ranged attraction around the periphery of the contact area while the deformation geometry is Hertzian as in the Figure 8a such that for a sperical tip and flat surface:

$$\begin{aligned} P &= \frac{Ka^3}{R_t} - 2\pi R_t\omega \\ \delta &= \frac{a^2}{R_t} \end{aligned} \tag{9}$$

where ω is the adhesion energy. Here, $\omega = \gamma_t + \gamma_s - \gamma_{ts} \approx 2\sqrt{\gamma_t\gamma_s}$ [23] with γ_t, γ_s and γ_{ts} are the tip, sample and tip-sample interface surface energies assuming no liquid layer between the tip and sample. If there is any liquid layer in the tip-sample interface, then $\omega \approx 2\gamma_L$ where γ_L is the liquid

surface tension. In air, if the tip and sample are hydrophilic, a thin water film layer exists on the sample and $\gamma_L = 72\ mJ/m^2$ is taken.

3) JKR Model: Adding the short-ranged adhesion forces, for spherical tip and flat surface as shown in Figure 8b, the JKR model results in the following equations:

$$P = \frac{Ka^3}{R_t} - \sqrt{3\pi\omega K a^3}$$
$$\delta = \frac{a^2}{R_t} - \frac{2}{3}\sqrt{3\pi\omega a/K}$$
$$a^3 = \frac{R_t}{K}\Big[P + 3\pi R_t\omega + \sqrt{6\pi R_t\omega P + (3\pi R_t\omega)^2}\Big] \quad (10)$$

4) MD Model: The MD model assumes a constant stress $\sigma_0 = 1.03/a_0$ over the annulus d as illustrated in Figure 8c. By analogy with the plastic zone ahead of a crack, the MD model can be used for all cases [19], [24], [8] such that:

$$1 = \frac{\lambda a^2}{2}\Big(\frac{K}{\pi R_t^2\omega}\Big)^{2/3}[\sqrt{m^2-1} + (m^2-2)cos^{-1}\frac{1}{m}] + \frac{4\lambda^2 a}{3}\frac{K}{\pi R_t^2\omega}^{1/3}[\sqrt{m^2-1}cos^{-1}\frac{1}{m} - m + 1]$$
$$\delta = \frac{a^2}{R_t} - \frac{4\lambda a}{3}\Big(\frac{\pi\omega}{R_t K}\Big)^{1/3}\sqrt{m^2-1}$$
$$P = \frac{Ka^3}{R_t} - \lambda a^2\Big(\frac{\pi\omega K^2}{R_t}\Big)^{1/3}[\sqrt{m^2-1} + m^2 cos^{-1}\frac{1}{m}]$$
$$\lambda = \frac{2.06}{a_0}\Big(\frac{R_t\omega^2}{\pi K^2}\Big)^{1/3} \quad (11)$$

where m is the ratio of the width of the annular region c to a. λ is a dimensionless parameter that is the ratio of the JKR theory contact area neck height to the intermolecular spacing a_0 [25]. It is also a measure of the elastic deformation of the surfaces to the effective range of surface forces. If $\lambda \to 0$, the MD model converges to the DMT model, and if $\lambda \to \infty$ it converges to the JKR model. For the contact of elastic spheres, an adhesion map can be constructed using the MD model for different values of λ and load. Johnson *et al.* [8] showed that the MD model can be replaced by the JKR model if $\lambda > 5.8$ or by the DMT model if $\lambda < 0.12$. For a given adhesion force P_a and load P, the MD model can be replaced by the Hertz model if $P > 20P_a$ [8].

5) Experiments and Simulations: For comparing the above deformation models, a silicon tip and silicon sample are brought into contact (assuming $E_{Si} = 135\ GPa$ and $\nu_{Si} = 0.35$). Assuming a water layer between the tip and sample, $\omega \approx 2\gamma_L$ where $\gamma_L = 72\ mJ/m^2$, and very smooth surfaces ($b \approx 0$), indentation force and contact radius a vs. z-displacement from the contact position Δ curves are obtained as shown in Figure 9 during unloading (retraction). In the figure, also the experimental unloading data with a slope of $8.5\ N/m$ are shown. However, the contact radius cannot be directly measured, and therefore experimental data is not shown. The results show that JKR overestimates the contact area while DMT and Hertz underestimates, and DMT and Hertz models also underestimates the applied load. For different samples with different E_s, the MD model gives the load, contact radius and m data as can be seen in Figure 10. As the surface becomes softer, i.e. E_s is smaller, the contact area is increased while the applied load is decreased. This may cause problems in the force feedback scaling since the same scaling factor can not give the sufficiently scaled feedback resolution and range on the operator finger for different surfaces with different hardness values. One solution is the preliminary calibration of the force scaling factor for all surfaces for optimal force feedback, and the other solution is using different AFM cantilevers with different stiffness, i.e. for soft surfaces small spring constant cantilevers, and for hard surfaces very stiff cantilevers. In our system, there are only two types of piezoresistive cantilevers available with the spring constants of around $1\ N/m$ and $8\ N/m$, and an initial calibration is realized for each surface which will be explained at below.

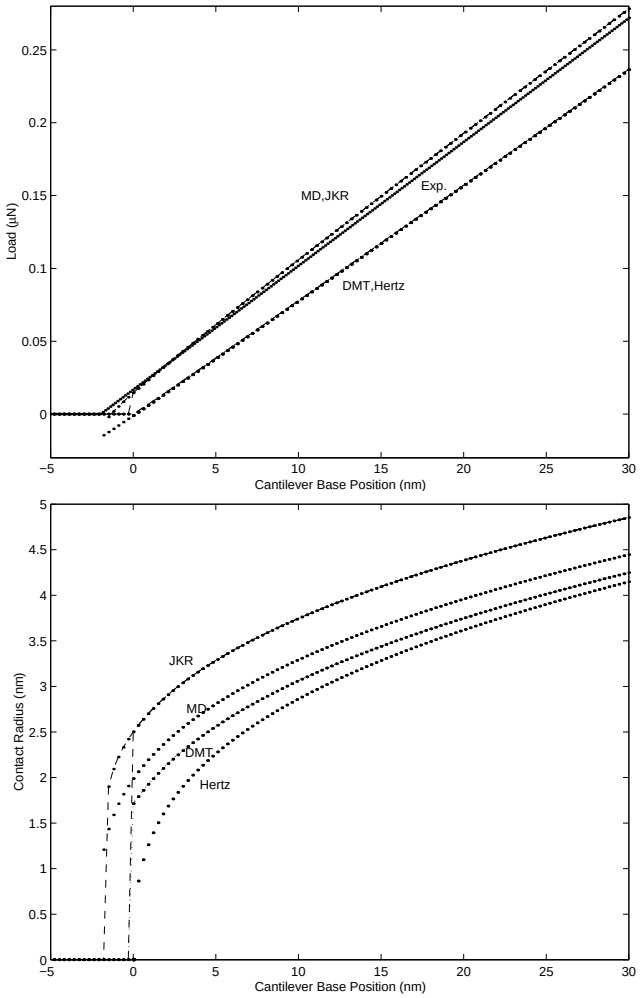

Fig. 9. Applied load and contact radius results for Hertz, DMT, JKR and MD models during unloading (retraction) in the case of a silicon tip and substrate contact (Exp. (dotted line) in the load graph represents the experimental data).

In the next experiment, a silicon AFM tip is touched to materials with different hardness values (single crystal silicon (100) with $E_s = 135\ GPa$, polyester with $E_s = 2\ GPa$, and silicone rubber (HSII, Dow Corning Inc.) with $E_s = 0.6\ MPa$), and the experimental unloading curves are obtained as shown in Figure 11. Depending on the E_s, the slope

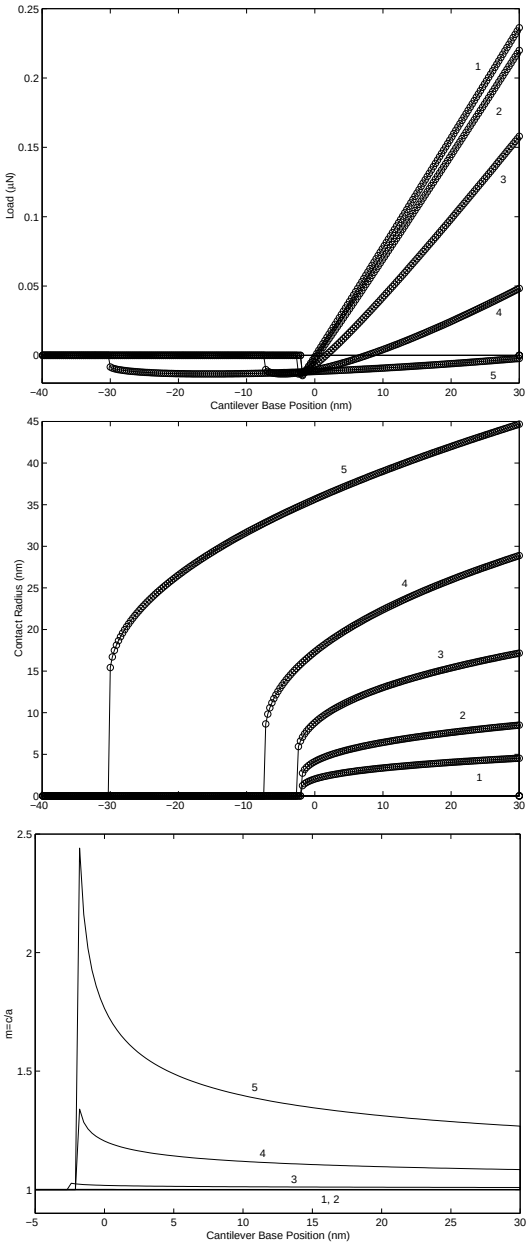

Fig. 10. Load (upper), contact radius (middle), and m (bottom) vs. tip base displacement curves for materials with different Young's moduli during unloading (E_s=(5) 0.01, (4) 0.1, (3) 1, (2) 10, (1) 100 GPa) using the MD model.

is different, i.e. larger E_s has a steeper slope, and the pull-off (separation) point gives information about the adhesion between the tip and surfaces.

IV. Scaled Bilateral Teleoperation Control

For feeling the scaled nanoforces on the human finger, the bilateral teleoperation control system shown in Figure 12 is constructed. In this 1-D force-reflecting servo type system, the operator controls the slave AFM nanoprobe z position while feeling the resulting scaled perpendicular nano scale forces in her/his finger using a bilateral controller. A 1 degree of freedom haptic device in Figure 13 [24] is used as the master device. The operator pushes the bar of the haptic device, and

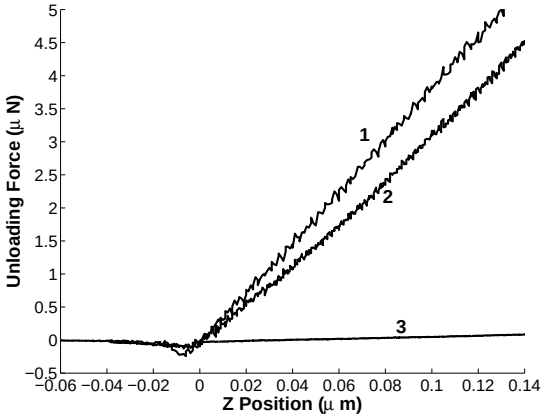

Fig. 11. Experimental unloading force and tip base displacement curves for: (1) silicon (100), $E_s = 135\ GPa$, (2) polyester, $E_s = 2\ GPa$, and (3) silicone rubber, $E_s = 0.6\ MPa$.

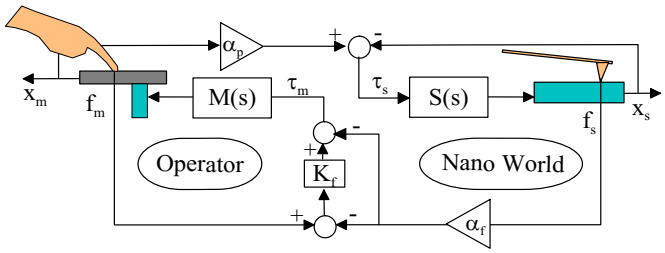

Fig. 12. Scaled bilateral teleoperation control system.

the applied operator force f_m, measured by a strain gage full bridge sensor, moves the bar down to a position x_m which is measured by a position sensor. Then, the nanoprobe z position x_s is controlled using a proportional-integral (PI) controller so that it can track the scaled master device position $\alpha_p x_m$. The new x_s position results in a nanoforce of f_s on the surface, and scaled nanoforce $\alpha_f f_s$ and master force difference is used to calculate the linear motor torque using a proportional-derivative (PD) controller. This torque enables the force feedback in the operator finger.

A. Dynamics Modeling

Force feedback is sensed through the linear motor torque with the master arm dynamics of:

$$m_m \ddot{x}_m + b_m \dot{x}_m = \tau_m + f_m \ , \tag{12}$$

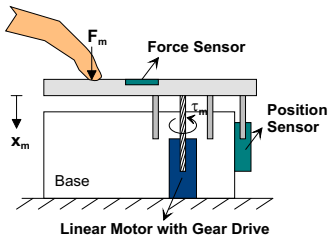

Fig. 13. Structure of the custom-made 1 degree of freedom haptic device with position and strain gauge force sensors for feeling the normal interatomic forces at the nanoscale.

with m_m is the arm mass, b_m is the damping ratio, f_m and x_m denote the operator force and arm position, and τ_m is the motor driving torque.

In the slave site, AFM tip base position (or sample position) $x_s(t)$ is controlled using Physick Instruments Co. (P-762.3L) piezoelectric stage with Linear Variable Differential Transformer (LVDT) integrated sensors. Closed-loop resolution is limited to $10\ nm$ due to the sensor resolution while in open-loop $1\ nm$ resolution is possible. The dynamics of the z-axis stage can be given as [26]:

$$\frac{1}{\omega_n^2}\ddot{x}_s + \frac{1}{\omega_n Q}\dot{x}_s + x_s = \tau_s - f_s \ , \tag{13}$$

where $\omega_n = 2\pi f_n$, $f_n = 450\ Hz$ is the resonant frequency, $Q = 20$ is the quality factor, x_s denotes the AFM cantilever base position, f_s is the force that the tip applies to the sample, and τ_s is the stage driving force.

The tip-sample interaction dynamics which is given in Eq. (3) can be written as:

$$f_s = k_c\zeta = -m_c^*\ddot{\zeta} + k_i x_s - k_i\zeta \ , \tag{14}$$

with $x_s = z$. Assuming quasi-static, i.e. slow, motion which means equilibrium at each x_s displacement:

$$f_s = \frac{k_i(x_s,\delta)k_c}{k_i(x_s,\delta) + k_c}x_s \ . \tag{15}$$

B. Control Scheme

The ideal response of the controller is given as follows [27]:

$$\begin{aligned} x_s &\rightarrow \alpha_p x_m \\ f_m &\rightarrow \alpha_f f_s \end{aligned} \tag{16}$$

at the steady state. Here $\alpha_f > 0$ and $\alpha_p > 0$ are the constant force and position scaling factors respectively. As the controller, a force-reflecting servo type controller is selected such that

$$\begin{aligned} \tau_m &= -\alpha_f f_s - K_f(\alpha_f f_s - f_m) \\ \tau_s &= K_v(\alpha_p\dot{x}_m - \dot{x}_s) + K_p(\alpha_p x_m - x_s) \end{aligned} \tag{17}$$

where K_p and K_v are proportional and differential control coefficients, and K_f is the force error gain. Using the slave and master dynamics equations, and assuming a very high tip-surface interaction stiffness such that $k_i >> k_c$, and $f_s = k_c x_s$, equalities for the ideal response at the steady state are given as follows:

$$\begin{aligned} \frac{x_s}{x_m} &= \alpha_p\frac{K_p}{1+K_p} \\ \frac{f_m}{f_s} &= \frac{1+K_p}{k_c\alpha_p K_f K_p} + \alpha_f\big(1+\frac{1}{K_f}\big) \ . \end{aligned} \tag{18}$$

Thus, for enabling the ideal responses, K_p and K_f should be selected as large as possible while they are upper bounded due to the stability conditions.

C. Selection of the Scaling Factors

In this paper, nanoforces and positions are linearly scaled with parameters α_f and α_p. For determining these parameters, there are different approaches. Recently, Goldfarb [28] concluded two cases: *Rule 1*: $\alpha_f = 1/\alpha_p = 1/l$ for structurally dominated interactions, *Rule 2*: $\alpha_f = 1/\alpha_p^2 = 1/l^2$ for surface-dominated interactions where $l = (x_s^{max} - x_s^{min})/(x_m^{max} - x_m^{min})$, and assuming $l >> 1$. Furthermore, for $\alpha_p = l$, we add a heuristic rule for the force scaling as

$$\alpha_f = \frac{f_m^{max} - f_m^{min}}{f_s^{max} - f_s^{min}} \ . \tag{19}$$

Upper max and min terms denote the minimum and maximum values for the given parameter. This kind of scaling could be especially useful for nanomanipulation cases where the resolution of the stages are limited for long ranges of tens of micrometers, and environmental disturbances largely reduce the measurement and positioning accuracy.

At first, the measurement limitations should be considered. For the positioning limits, resolution $\delta_p = 10\ nm$ in the closed-loop control case is taken. Denoting the initial height of the tip above the sample surface as L, and a maximum indentation depth as δ_{max}, then $x_s^{max} - x_s^{min} = L + \delta_{max}$. The deflection of the cantilever is limited by the electronics such that $-10S \le \zeta \le 10S$ where S is the conversion term for the deflection from $Volt$ to μm. It is calibrated before the experiments (in our case $S = 0.033\ \mu m/V$). Thus, $\delta_{max} \le 10S = 0.33\ \mu m$.

For the nanoforce measurements, the thermal and electrical noise in the piezoresistive cantilever deflection measurement system, e_c, is peak-to-peak $50\ mV$ which means an approximate force resolution of $\delta_f = 0.05k_cS = 13\ nN$. Since ζ is limited, also $-10k_cS \le f_s \le 10k_cS$. For $k_c = 8\ N/m$, $-2.6\ \mu N \le f_s \le 2.6\ \mu N$. However, the attractive nanoforces are relatively very small as compared to contact forces, and typically $-0.6\ \mu N \le f_s \le 2.6\ \mu N$. Furthermore, due to δ_p, minimum ζ steps are limited to $k_c\delta_p = 80\ nN$. Thus, the overall force resolution in the closed-loop control case is $\delta_f = 80\ nN$. On the other hand, for the open-loop control, there is no limitation from δ_p, and $\delta_f = 13\ nN$.

The resolutions and ranges can be combined for determining the possible number of control steps N_f and N_p for the nanoforce and position as follows:

$$\begin{aligned} N_p &= \frac{L + \delta_{max}}{\delta_p} \\ N_f &\le 20k_c\frac{S}{\delta_f} \ . \end{aligned} \tag{20}$$

For the case of $\delta_{max} = 0.3\ \mu m$ and $L = 0.1\ \mu m$, $N_p = 40$ and $N_p = 400$, and $N_f = 67$ and $N_f = 400$ for the $\delta_p = 10\ nm$ and $\delta_p = 1\ nm$ cases using above values. For an accurate control and sensitive feedback, N_p and N_f should be as large as possible. Therefore, $10\ nm$ resolution would not be sufficient for precise feedback, and $1\ nm$ resolution should be utilized.

For the master device, the motion range is limited to $2\ cm$ with $\delta_p = 0.004\ cm$. Thus, $N_p = 500$ for the master positioning which is assumed to be sufficient. Force measurement

resolution is $\delta_f = 0.02\ N$ for the strain gauge sensors including the electrical noise, and the maximum measurable range is approximately $\pm 5\ N$. Thus, $N_f \leq 500$ which is also assumed to be sufficient. Finally,

$$\alpha_p = (L + \delta_{max})/2.0 \times 10^{-4}$$
$$\alpha_f = (f_m^{max} - f_m^{min})/3.2 \times 10^6\ . \quad (21)$$

V. Virtual Reality Simulator and System Setup

For simulating the nanoscale touch feedback, a VR simulator is constructed for freely changing the physical parameters, and initial training. In the 3-D graphics interface, probe tip position and traces are displayed in real-time while the scaled nanoforces are felt through the haptic device. A realistic simulator would enable a real-time animator display for real-time nanomanipulation monitoring such that the models could predict the position of the manipulated objects in real-time, and could *animate* this modelled behavior in the simulator. Using the haptic device, and the nanoscale contact mechanics models, hybrid simulation type of touching experiments are realized.

During the experiments, a custom-made AFM system is utilized [29],[4]. The overall hardware setup of the experiments can be seen in Figure 14. A real-time Linux operation system is used with 3 ms bandwidth for AFM system, haptic device and teleoperation control. The AFM tip position on the off-line 3-D surface AFM image is shown with the same bandwidth update. All signals are recieved and sent using A/D and D/A boards with high speed (around 10 KHz). Communication between the teleoperation system and visual display Silicon Graphics workstation (IRIX-Indigo II) is held by 10 Mbps Ethernet link.

In the experiments, the surface is scanned by the AFM probe in the contact or tapping mode to get its 3-D image. This image is sent to the VR graphics display, and the operator chooses the most suitable orientation and magnification of the image. Then, using the haptic device (for z-motion) and mouse (for $x-y$ motion), the operator controls the motion of the AFM probe while feeling the scaled nanoforces in her/his finger using the force reflecting servo-type controller and seeing the real-time AFM tip position and touch on the surface on the VR display.

For the simulations, the AFM setup is replaced by the theoretical nanoforce models given in Section III, and the operator virtually touches to a given surface while feeling the simulated scaled nanoforces.

VI. Experiments

A. AFM Imaging

At first, the custom-made AFM system is tested for getting nanoscale 3-D topology images. As an example, a silicon substrate (TGT-01 grating, Silicon-MDT Inc.) with 300 nm height sharp conical tips is scanned in the tapping mode imaging mode as shown in Figure 15. From the image, it can be seen that topologies down to tens of nanometer can be observed with our AFM setup.

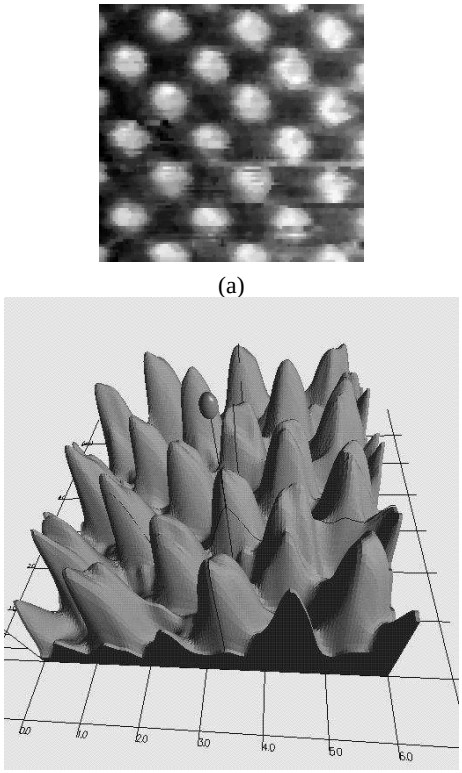

Fig. 15. Experimental AFM topology image ($6 \times 6 \times 0.3\ \mu m^3$ size) of sharp silicon tips by the custom-made AFM: (a) 2-D grey scale image, and (b) 3-D Virtual Reality graphics image (spherical ball on the surface displays the 3-D real-time position of the AFM nanoprobe tip).

B. Single-Asperity Contact Feedback

For the teleoperated point touch to a surface using the AFM tip and the custom-made haptic device, a low-speed approach and retraction of the cantilever tip to a mica sample by the control of sinusoidal operator force is simulated by the force-position teleoperation control approach. In this simulation, the slave controller is open-loop and $x_s = \alpha_p x_m$ is assumed to be held all the time. From the Figure 16, the master and slave forces converge to the same value which means that the controller enables a reliable feedback. The simulation parameters are $\alpha_p = 15 \times 10^{-9}$, $\alpha_f = 4 \times 10^6$, $M_m = 0.1\ kg$, $B_m = 100\ Ns/m$, $K_f = 100$, $H = 1 \times 10^{-19}\ J$, $R_t = 25\ nm$, $a_0 = 3.49\ A^o$, $E = 0.05\ GPa$, $\nu = 0.3$, and $k_c = 30\ N/m$. Also a white noise with the zero mean and 0.001 variance is added for simulating the operator force measurement noise by the strain gauges.

As an example of the teleoperated nanoscale touch experiment results, silicon AFM tip approached and retracted from a silicon (100) flat substrate. The AFM probe parameters are $R_t = 20\ nm$, $k_c = 8\ N/m$ and $S = 0.033\ \mu m/V$. Touching to the silicon sample at the 40% humidity conditions, resulting master and scaled slave position and forces can be seen in Figure 17. Experimental parameters are $K_f = 2$, initial tip height $L = 0.6\ \mu m$, $\alpha_p = 4 \times 10^{-3}$ and $\alpha_f = 2.0 \times 10^6$. As can be seen from the figure, ideal responses of tracking the master and scaled slave forces and positions are realized successfully. The negative attractive forces are significantly

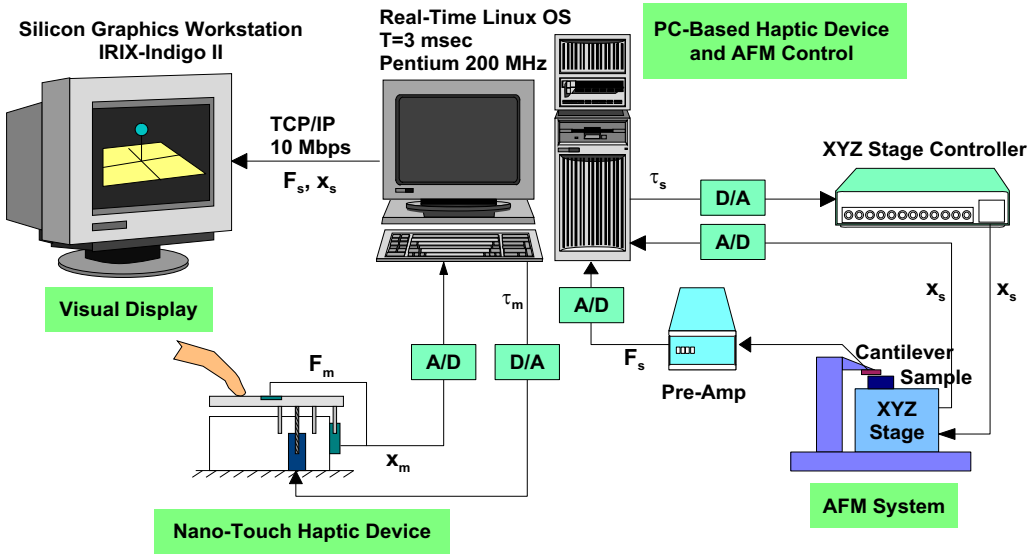

Fig. 14. Experimental system setup for the teleoperated nanoscale touch feedback applications using the custom-made AFM and 1 d.o.f. haptic device.

large enough to feel the sticking to the surface. However, this sticking effect is small during the approach, and very large when retracting back. The reason is the adhesion force which results in an increased attractive force during separation. This difference causes of the force tracking error during the approach phases since the force occurs only very close to the surface ($20 - 50\ nm$). However, there is almost no tracking error for the positions since the piezoelectric z stage and the haptic device have the same bandwidth of $33\ Hz$, and z stage is controlled in closed-loop.

C. Surface Tactile Feedback

In this experiment, surface forces and topographies are felt on the operator's hand while moving on the sample surface in $x-y$ coordinates. At first, the cantilever tip is approached to the surface, and put in contact with the substrate. Then, by controlling the $x-y$ AFM cantilever motion, the operator can feel the contact nanoforces and surface topography by the bilateral teleoperation controller during the $x-y$ motion. As the experimental result, silicon square gratings (TGZ-03 grating, Silicon-MDT Inc.), which are seen in the optical microscope top view image as in Figure 18a, is scanned along the line shown in the figure. The resulting tactile-sensing with the scale parameters of $\alpha_p = 10^{-6}$ and $\alpha_f = 1\times10^{6}$, and the force error gain of $K_f = 10$ is given in Figure 18b. The upward jumps stand for the silicon grid structures of $480\ nm$ height. Here, the nanoobjects are assumed to be fixed on the substrate since the touching operation could move the non-fixed nanoobjects on the substrate by the applied pushing/pulling forces. However, if the objects are not completely fixed, the same operation could be utilized to manipulate them.

As another tactile feedback mode, the force feedback is turned off, and just the measured 3-D surface topography is sensed at the operator's hand while moving on the sample surface in $x-y$ coordinates. Here, AFM z position is controlled in real-time for constant contact force control, and held z position at each $x-y$ position is scaled, and sent to the teleoperation controller. Quantum dot structures with 10-30 nm diameter sizes are felt along the scanned line as shown in Figure 19.

VII. Discussions

From the experimental and simulation results, it can be observed that the proposed bilateral scaled teleoperation control system is successful for providing tactile and force feedback at the nanoscale. The important parameters for the repeatable and stable touch feedback are as follows:

- Scanning speed: taking the bandwidth effect problem into consideration [1], the scanning speed should be small for feeling the small features reliably.
- The stage closed-loop positioning accuracy is around $10\ nm$ during the experiments which added limitations to the resolution of the felt nanoforces. This sometimes caused instability problems in the case of very hard surfaces where vibration could occur if a large K_f is selected. Therefore, the accuracy of the stage should be increased to the sub-nanometer level for more stable and high resolution force feedback.
- Selection of α_f force scaling factor: For high surface adhesion, i.e. large tip radius (R_t) and high adhesion energy, $\alpha_f = 1/\alpha_p$, and for small adhesion forces, $\alpha_f = 1/\alpha_p^2$ could give a better force feedback from the theoretical calculations of Goldfarb [28]. However, depending on the softness of the samples, these rules would not apply since the interaction forces could become exponentially very small while the motion range increases. Thus, our proposed heuristic rule becomes more attractive where the minimum and maximum contact force values, and motion ranges are measured before the experiments, and α_f is selected according to the Eq. (19).
- Electrostatic forces could be negligible for previously non-charged surfaces and grounded substrates. However, for a non-conducting sample, even if the tip is conductive or semi-conductive, charges can be generated during the contact interaction which can result in increased

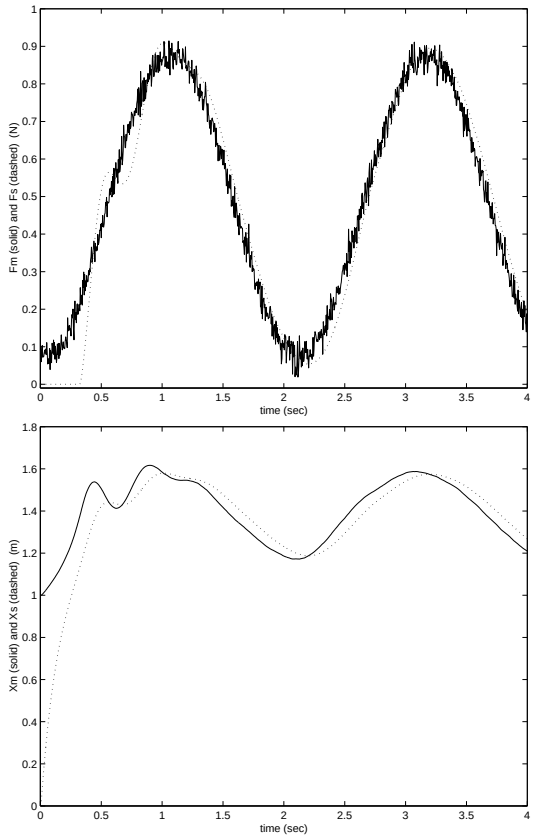

Fig. 16. Simulated scaled slave (dotted line) and master (solid-line) forces (upper), and positions (lower) during approaching to a mica sample by the control of a sinusoidal operator force.

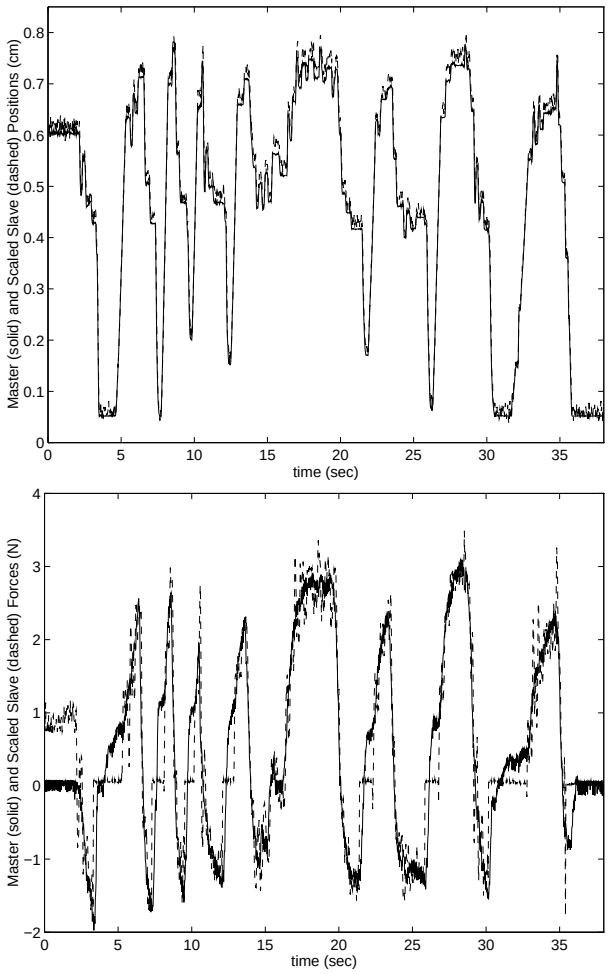

Fig. 17. Touching results to a flat silicon sample with a silicon tip: master (solid) and scaled slave (dashed) position (upper) and forces (lower). In the force plot, negative forces correspond to the attractive approach or separation forces while positive ones do the repulsive contact forces.

electrostatic forces by time. Furthermore, adhesion forces can increase over time as the tip could wear and R_t could change during the contact interaction. Thus, the adhesion forces could be *time dependent* which should be included in the nanoscale touch feedback simulator models [30].

- During the approach process, non-contact forces become large only in the close vicinity to the surface. Therefore, the approach speed should be slow and the positioning accuracy of the stage should be high for a *repeatable* approach nanoforce feedback. Thus, in the experiments, approaching non-contact forces are felt only sometimes with $10\ nm$ positioning accuracy. As a possible solution to these kinds of cases: α_f could be selected depending on the region such as approaching, indenting and retracting regions. However, in this case, the continuity of the felt nanoforces would be a difficult issue during passing from one region to another.
- Water layer on the surfaces and tip can cause the instable jump-in-contact problem when approaching surfaces with soft cantilevers if $dF_{non-con}/dh = k_i > k_c$, and increases the adhesion meniscus bridge length during the retraction. Therefore, for hard surfaces with water layer, hard cantilevers (high k_c) should be selected for preventing these unstable problems.
- Cantilever parameters such as the force constant k_c, tip size R_t and shape, resonant frequency f_r, and quality factor Q_c should be measured for each probe to be used in the experiments for realistic theoretical predictions.

Proposed force modelling is put into the VR nanoscale touch feedback simulator which enables a simulated training and test environment. At the simulations, also the effect of all different contact mechanics models can be tested easily. Frictional models are also added for a 2-D Simulator [31], and, as a future work, by changing the simulator graphics to 3-D, also the 3-D simulations would be possible [32].

VIII. Conclusions

In this paper, a teleoperated nanoscale touching system is proposed, and nanocontact mechanics models are introduced. Using a 1 degree of freedom haptic device, and force-reflecting servo type scaled teleoperation controller, preliminary touching experiments and simulations are realized. The MD contact model gives the best results in the Virtual Reality based nanoscale touch feedback simulator experiments since it can be applied to all cases without any assumption. Scaling issue of the nanoscale forces and positions is discussed and possible solutions are proposed. Experimental and simulation results

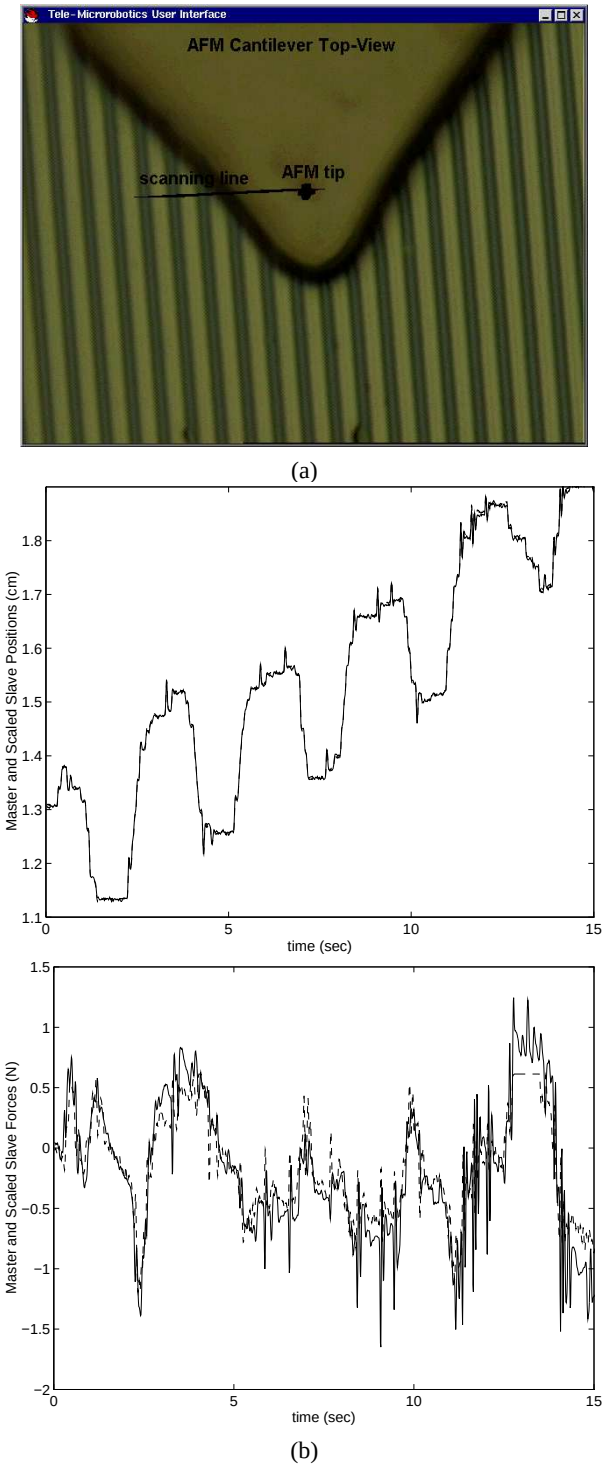

Fig. 18. (a) Silicon grids with $480\ nm$ height and $3\ \mu m$ pitch are felt along the black line, and (b) resulting topology and force feedback using the force reflecting servo type controller: scaled slave (dashed line) and master (solid line) positions (upper) and forces (lower).

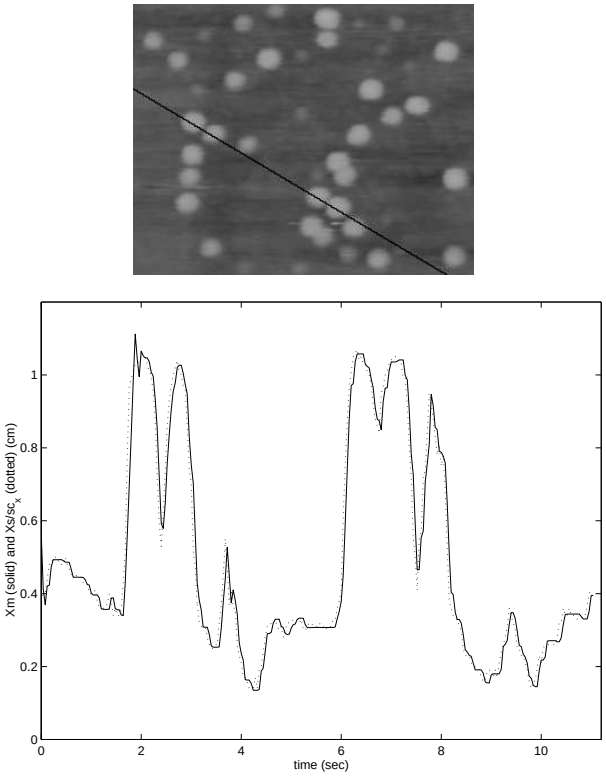

Fig. 19. Feeling the InAs quantum dots with diameters around $10-30\ nm$ along the scanned line (upper image), and the resulting topology feedback (lower image): resulting master (solid) and scaled slave positions (dotted).

show that the proposed system can be used for nanoscale touching applications. During the experiments it is observed that only visual feedback is not sufficient for interacting in the nano world since the visual feedback includes many source of errors such as positioning drifts, nonlinearities, noises, etc., and there is no real-time nanoscale visual feedback possibility at present in air. Therefore, real-time force feedback is one of the promising solutions for compensating these errors.

As future works, a novel 3 degree of freedom haptic device specific to the nanoscale force feedback applications would be constructed where the AFM system would also enable frictional force feedback. Furthermore, biological object manipulation experiments would be realized for sensing their elasticity and viscoelasticity, and mechanical manipulation tasks such as cutting, pushing, etc. In the biological application case, operation environment becomes liquid, and the proposed non-contact force models will be changed accordingly by eliminating capillary and electrostatic forces and adding hydrophobic, steric, double-layer, etc. type of new force models.

ACKNOWLEDGEMENTS

Authors would like to thank Satoshi Horiguchi for helping with the Virtual Reality graphics software and interface, Hiroyuki Fujita for his comments and discussions, and Yasuhiko Arakawa for quantum dot samples and his comments.

REFERENCES

[1] M. Sitti and H. Hashimoto, "Tele-nanorobotics using Atomic Force Microscope as a robot and sensor," *Advanced Robotics*, vol. 13, no. 4, pp. 417–436, 1999.

[2] A. Requicha, C. Baur, A. Bugacov, and et al., "Nanorobotic assembly of two-dimensional structures," *Proc. of the IEEE Int. Conf. on Robotics and Automation*, pp. 3368–3374, Leuven, Belgium, 1998.
[3] M. Guthold, M. Falvo, W. Matthews, S. Paulson, and et al., "Controlled manipulation of molecular samples with the nanoManipulator," *IEEE/ASME Trans. on Mechatronics*, vol. 5, pp. 189–198, June 2000.
[4] M. Sitti and H. Hashimoto, "Controlled pushing of nanoparticles: Modeling and experiments," *IEEE/ASME Trans. on Mechatronics*, vol. 5, pp. 199–211, June 2000.
[5] M. Sitti, "Teleoperated 2-D micro/nanomanipulation using Atomic Force Microscope," *Ph.D. Thesis*, Dept. of Electrical Engineering, University of Tokyo, Tokyo, Sept. 1999.
[6] M. Sitti, "Survey of nanomanipulation systems," *IEEE Nanotechnology Conference*, pp. 75–80, Maui, USA, 2001.
[7] N. A. Burnham and A. J. Kulik, "Surface forces and adhesion," *Handbook of Micro/Nanotribology*, ed. by B. Bhushan, CRC Press, Dec. 1997.
[8] K. Johnson and J. Greenwood, "An adhesion map for the contact of elastic spheres," *J. of Colloid and Interface Science*, vol. 192, pp. 326–333, 1997.
[9] B. Brushan, *Micro/Nanotribology and Its Applications*, Kluwer Academic Pub., Vol. E330, 1997.
[10] W. Kiridena, V. Jain, P. Kuo, and G.-Y. Liu, "Nanometer-scale elasticity measurements on organic monolayers using Scanning Force Microscopy," *Surface and Interface Analysis*, vol. 25, pp. 383–389, June 1997.
[11] H. Rafi-Tabar, "Nanoscopic modelling of the adhesion, indentation and fracture characteristics of metallic systems via molecular dynamics simulations," *Computational Materials Design*, pp. 36–48, ed. by Kitagawa, H., Aihara, T. Jr., Kawazoe, Y., Springer, Berlin, 1998.
[12] M. R. VanLandingham, S. H. McKnight, and et al., "Relating elastic modulus to indentation response using Atomic Force Microscopy," *J. of Materials Science Letters*, vol. 16, pp. 117–119, 15 Jan. 1997.
[13] M. Sitti and H. Hashimoto, "Two-dimensional fine particle positioning using a piezoresistive cantilever as a micro/nano-manipulator," *Proc. of the IEEE Int. Conf. on Robotics and Automation*, pp. 2729–2735, Detroit, USA, May 1999.
[14] J. Tamayo and R. Garcia, "Deformation, contact time, and phase contrast in tapping mode Scanning Force Microscopy," *Langmuir*, vol. 12, no. 18, pp. 4430–4435, 1996.
[15] R. W. Stark, S. Thalhammer, and et al., "The AFM as a tool for chromosomal dissection - the influence of physical parameters," *Appl. Phys. A*, vol. 66, pp. 579–584, 1998.
[16] D. Sarid, J. P. Hunt, R. K. Workman, and et al., "The role of adhesion in tapping-mode Atomic Force Microscopy," *Appl. Phys. A*, no. 66, pp. 283–286, 1998.
[17] D. Maugis, *Contact, adhesion, and rupture of elastic solids*, Springer Verlag Pub., New York, 2000.
[18] N. A. Burnham, O. Behrend, and et al., "How does a tip tap?," *Nanotechnology*, vol. 8, pp. 67–75, 1997.
[19] D. Maugis, "Adhesion of spheres: The JKR-DMT transition using a Dugdale model," *J. of Colloidal and Interface Science*, vol. 150, pp. 243–269, April 1992.
[20] R. L. Hollis, S. Salcudean, and D. W. Abraham, "Toward a tele-nanorobotic manipulation system with atomic scale force feedback and motion resolution," *Proc. of the IEEE Int. Conf. on MEMS*, pp. 115–119, 1990.
[21] M. Falvo, R. Superfine, S. Washburn, and et al., "The nanoManipulator: A teleoperator for manipulating materials at the nanometer scale," *Proc. of the Int. Symp. on the Science and Technology of Atomically Engineered Materials*, pp. 579–586, Richmond, USA, Nov 1995.
[22] D. R. Baselt, G. U. Lee, K. M. Hansen, L. A. Chrisey, and R. J. Colton, "A high-sensitivity micromachined biosensor," *Proc. IEEE*, vol. 85, no. 4, pp. 672–680, 1997.
[23] J. Israelachvili, *Intermolecular and Surface Forces*, 2nd Ed., Academic Press, London, 1992.
[24] M. Sitti and H. Hashimoto, "Tele-nanorobotics using Atomic Force Microscope," *Proc. of the IEEE/RSJ Int. Conf. on Intelligent Robots and Systems*, pp. 1739–1746, Victoria, Canada, Oct. 1998.
[25] Y. Zao and T. Yu, "Failure modes of MEMS and microscale adhesive contact theory," *Int. J. of Nonlienar Sciences and Numerical Simulation*, vol. 1, pp. 361–371, 2000.
[26] T. R. Hicks and P. D. Atherton, *The Nano Positioning Book*, Queensgate Inst. Ltd., UK, 1997.
[27] Y. Yokokohji and T. Yoshikawa, "Bilateral control of master-slave manipulators for ideal kinesthetic coupling–formulation and experiment," *IEEE Trans. on Robotics and Automation*, vol. 10, pp. 605–619, Oct. 1994.
[28] M. Goldfarb, "Dimensional analysis and selective distortion in scaled bilateral telemanipulation," *Proc. of the IEEE Int. Conf. on Robotics and Automation*, pp. 1609–1614, Leuven, Belgium, 1998.
[29] M. Sitti and H. Hashimoto, "Two-dimensional fine particle positioning under optical microscope using a piezoresistive cantilever as a manipulator," *Journal of Micromechatronics*, vol. 1, no. 1, pp. 25–48, 2000.
[30] J. Chen, C. Dimattia, and et al., "Sticking to the point: A friction and adhesion model for simulated surfaces," *Proc. of the Annual Symp. on Haptic Interfaces for Virtual Env. and Teleoperator Systems*, pp. 167–171, 1997.
[31] M. Sitti, "Nanotribological characterization system by AFM based controlled pushing," *IEEE Nanotechnology Conference*, pp. 99–104, Maui, USA, 2001.
[32] M. Sitti, B. Aruk, K. Shintani, and H. Hashimoto, "Scaled teleoperation system for nanoscale interaction and manipulation," *Advanced Robotics*, vol. 17, 2003 (to appear).

Metin Sitti received the BSc and MSc degrees in Electrical and Electronic Engineering from Bogazici University, Istanbul, Turkey, in 1992 and 1994 respectively, and the PhD degree in Electrical Engineering from the University of Tokyo, Tokyo, Japan, in 1999. He worked in the CAD/CAM Robotics Department in the TUBITAK Marmara Research Center, Kocaeli, Turkey, as a research engineer during 1994-1996, working on visual servoing, computer vision, and robot control projects. He was a recipient of the Monbusho Research Fellowship during his study in Japan. He was a research scientist and lecturer at the Department of Electrical Engineering and Computer Sciences, University of California, Berkeley during 1999-2002 working on micromechanical flying insect robots and biomimetic gecko foot-hair micro/nanostructure analysis and fabrication. He is currently an assistant professor at the Department of Mechanical Engineering and the Robotics Institute, Carnegie Mellon University. His research interests include micro/nano-robotics, nanomanufacturing, biomimetic micro/nano systems, bio-nanotechnology, Scanning Probe Microscopy, haptic interfaces, and tele-robotics. He received the best paper award in the IEEE/RSJ International Conference on Intelligent Robots and Systems in 1998, and the best video award in the IEEE Robotics and Automation Conference in 2002. He is a member of IEEE, ASME, and Robotics Society of Japan.

Hideki Hashimoto received the BSc, MSc and DrEng degrees in Electrical Engineering from the University of Tokyo, Tokyo, Japan, in 1981, 1984 and 1987, respectively. He is currently an Associate Professor with the Institute of Industrial Science, University of Tokyo. From 1989 to 1990, he was a Visiting Scientist in the Laboratory for Information and Decision Systems and the Laboratory for Electromagnetics and Electronics Systems at the Massachusetts Institute of Technology, Cambridge, MA. His research interests are in the areas of robotics, control, intelligent transportation systems, and human-machine interfaces. He is an active member of the IEEE Industrial Electronics and IEEE Robotics and Automation Societies, has served on the Administrative Committees of both. He is also a member of the Japanese Society of Instrument and Control Engineers, Institute of Electrical Engineers of Japan, and Robotics Society of Japan.